eNeuro

Study of the Size and Shape of Synapses in the Juvenile Rat Somatosensory Cortex with 3D Electron Microscopy

Andrea Santuy[1], J. R. Rodríguez[1,2], Javier de Felipe[1,2] and Angel Merchan-Perez[1,3]

[1]*Laboratorio Cajal De Circuitos Corticales, Centro De Tecnología Biomédica, Universidad Politécnica De Madrid. Pozuelo De Alarcón, Madrid, 28223, Spain*

[2]*Instituto Cajal, Consejo Superior De Investigaciones Científicas, Madrid, 28002, Spain*

[3]*Departamento De Arquitectura y Tecnología De Sistemas Informáticos, Universidad Politécnica De Madrid. Boadilla Del Monte, Madrid, 28660, Spain*

1 **Study of the size and shape of synapses in the juvenile**

2 **rat somatosensory cortex with 3D electron microscopy**

3

4 Abbreviated Title : Size and shape of synapses in the cortex

5 **Santuy, A.[1], Rodríguez, J.R.[1, 2], DeFelipe, J.[1, 2], Merchan-Perez, A.[1, 3]**

6 [1] Laboratorio Cajal de Circuitos Corticales, Centro de Tecnología Biomédica, Universidad

7 Politécnica de Madrid. Pozuelo de Alarcón, 28223, Madrid, Spain.

8 [2] Instituto Cajal, Consejo Superior de Investigaciones Científicas, 28002, Madrid, Spain.

9 [3] Departamento de Arquitectura y Tecnología de Sistemas Informáticos, Universidad Politécnica

10 de Madrid. Boadilla del Monte, 28660, Madrid, Spain.

11

12

15

16

17 **Correspondence should be addressed to** Angel Merchan-Perez, Laboratorio Cajal de

18 Circuitos Corticales, Centro de Tecnología Biomédica, Universidad Politécnica de Madrid.

19 Pozuelo de Alarcón, 28223, Madrid, Spain. amerchan@fi.upm.es

20

21 **Number of Figures:** 7

22 **Number of Tables:** 3

23 **Number of Multimedia: 0**

24 **Number of words for Abstract:** 149

25 **Number of words for Significance Statement:** 120

26 **Number of words for Introduction:** 736

27 **Number of words for Discussion:** 2524

28

Study of the size and shape of synapses in the juvenile rat somatosensory cortex with 3D electron microscopy

Abstract

Changes in the size of the synaptic junction are thought to have significant functional consequences. We used focused ion beam milling and scanning electron microscopy (FIB/SEM) to obtain stacks of serial sections from the six layers of the rat somatosensory cortex. We have segmented in three-dimensions a large number of synapses (n=6891) to analyze the size and shape of excitatory (asymmetric) and inhibitory (symmetric) synapses, using dedicated software. This study provided three main findings. Firstly, the mean synaptic sizes were smaller for asymmetric than for symmetric synapses in all cortical layers. In all cases, synaptic junction sizes followed a log-normal distribution. Secondly, most cortical synapses had disc-shaped postsynaptic densities (93%). A few were perforated (4.5%), while a smaller proportion (2.5%) showed a tortuous horseshoe-shaped perimeter. Thirdly, the curvature was larger for symmetric than for asymmetric synapses in all layers. However, there was no correlation between synaptic area and curvature.

Significance Statement

The size of synapses correlates with functional aspects such as the probability of neurotransmitter release or the number of postsynaptic receptors. The data obtained in the present study is based on the analysis of thousands synaptic junctions, that have been imaged and segmented in 3D with semi automated electron microcopy and image analysis methods, providing a robust set of morphological data. Since currently-available 3D quantitative data are scarce and mainly based on individual cases, the present results in conjunction with other crucial microanatomical data —such as the number and distribution of different types of synapses and the identification of postsynaptic targets in different cortical layers— will help to better understand the structure of microcircuits and to build realistic cortical models.

Introduction

There are two main types of chemical synapses in the cerebral cortex that can be identified at the electron microscope level based on morphological criteria: asymmetric synapses (AS), that have a thickened postsynaptic density (PSD) and are generally excitatory (glutamatergic), and symmetric synapses (SS), that have a thinner PSD and are inhibitory (GABAergic) (Houser et al., 1984; Peters et al., 1991; Ascoli et al., 2008). In the cerebral cortex, the vast majority of synapses are established in the neuropil which represents 90−98% of the volume of the gray matter (Alonso-Nanclares et al., 2008). In the neuropil, which is composed of dendrites, axons and glial processes, most cortical synapses are excitatory (80−90%) and originate from spiny neurons and extrinsic cortical afferents. Inhibitory synapses are less numerous (about 10−20%) and mainly originate from local interneurons (Feldman, 1984; Beaulieu and Colonnier, 1985; Schüz and Palm, 1989; White and Keller, 1989; DeFelipe and Fariñas, 1992; DeFelipe et al., 2002; White, 2007; Silberberg, 2008).

Synapses are dynamic structures than can undergo modifications due to variations in their activity patterns; they are continuously remodeled and replaced as part of the normal maintenance of the brain (Fauth and Tetzlaff, 2016; Lisman, 2017). This is important because the size of the active zone (AZ) is proportional to the number of docked synaptic vesicles and to the probability of neurotransmitter release (Schikorski and Stevens, 1997; Branco et al., 2010; Matz et al., 2010; Holderith et al., 2012), and the PSD area is proportional to the number of postsynaptic receptors (Nusser et al., 1998; Kharazia and Weinberg, 1999; Takumi et al., 1999; Ganeshina et al., 2004a, b; Tarusawa et al., 2009). Thus, changes in the surface areas of the AZ and PSD have significant functional consequences. However, measuring the size of a synapse is not an easy task and different approaches have been used to overcome this difficulty. The cross-sectional length of the PSDs in single photomicrographs obtained by transmission electron microscopy (TEM) gives a rough estimate of synaptic sizes (DeFelipe et

4

96   al., 1999). Better estimates can be obtained from TEM serial sections, measuring the maximum

97   width of the PSDs (Tarusawa et al., 2009) or the PSD surface area (Toni et al., 2001). However,

98   serial sectioning is a time-consuming and technically demanding task. Consequently, data on

99   synaptic sizes are either relatively inaccurate or based on relatively scant data. Recently, new

100   electron microscopy techniques have been developed that allow us to obtain long series of

101   sections in an automated way (Denk and Horstmann, 2004; Smith, 2007; Knott et al., 2008;

102   Merchan-Perez et al., 2009; Helmstaedter, 2013; Morgan and Lichtman, 2013). For example,

103   using focused ion beam milling and scanning electron microscopy (FIB/SEM), large numbers of

104   synaptic junctions can be three-dimensionally segmented from serial sections (Morales et al.,

105   2011). Simple measurements, such as the Feret's diameter (the diameter of the smallest

106   sphere circumscribing the three-dimensional object) can be obtained (Anton-Sanchez et al.,

107   2014; Merchan-Perez et al., 2014). The main advantage of Feret's diameter is its simplicity,

108   although it provides no information about shape. A more accurate method has been

109   developed to estimate the size and shape of synapses. Since the AZ and the PSD are located

110   face to face and their surface areas are very similar (Schikorski and Stevens, 1997, 1999) they

111   can be represented by a single surface, the synaptic apposition surface (SAS), that can be

112   automatically extracted with dedicated software (Morales et al., 2013). The SAS provides not

113   only quantitative information, but also qualitative visual information about the shape of the

114   synaptic junction, such as curvature, perimeter tortuosity or the presence of perforations.

115   In this work, we have studied the size and shape of AS and SS on spines and dendritic shafts in

116   the neuropil of all cortical layers of the somatosensory cortex. We used a large database of

117   synaptic junctions that were fully segmented in 3D (n= 6891) from Wistar rats at postnatal day

118   14. We extracted and measured the SAS of these synapses using the method developed by

119   Morales et al (2013). This experimental animal —at this age—was selected since we intended

120   to integrate these data with other anatomical, molecular, and physiological data that have

121   already been collected from the same cortical region. The final goal is to obtain accurate

122 quantitative data that help to create a detailed, biologically accurate model of circuitry for all

123 layers in the primary somatosensory cortex, within the framework of the Blue Brain Project

124 (Markram et al., 2015).

125 **Materials and methods**

126 *Animals and Tissue Preparation*

127

128 Three male Wistar rats sacrificed on postnatal day 14 were used for this study. Animals were

129 administered a lethal intraperitoneal injection of sodium pentobarbital (40 mg/kg) and were

130 intracardially perfused with 2% paraformaldehyde and 2.5% glutaraldehyde in 0.1 M

131 phosphate buffer (PB). The brain was then extracted from the skull and processed for electron

132 microscopy according to a previously described protocol (Merchan-Perez et al., 2009). Briefly,

133 the brains were extracted from the skull and post-fixed at 4°C overnight in the same solution.

134 Vibratome sections were obtained (150 μm thick). Sections containing the primary

135 somatosensory cortex (hindlimb representation) were selected with the help of an atlas

136 (Paxinos and Watson, 2007). The sections were then osmicated for 1 h at room temperature in

137 PB with 1% OsO4, 7% glucose and 0.02 M CaCl2. After washing in PB, the sections were stained

138 *en bloc* for 30 min with 1% uranyl acetate in 50% ethanol at 37°C, and were then flat-

139 embedded in Araldite. These tissue samples have been used previously to describe the

140 proportions and densities of AS and SS synapses on spines and dendritic shafts across all

141 cortical layers, as well as the occurrence of single or multiple synapses on the same spine

142 (Santuy et al., 2017).

143 All animals were handled in accordance with the guidelines for animal research set out in the

144 European Community Directive 2010/63/EU, and all procedures were approved by the local

145 ethics committee of the Spanish National Research Council (CSIC).

146

147   *Three-Dimensional Electron Microscopy*

148

149   Three-dimensional brain tissue samples of the somatosensory cortex (hindlimb representation)

150   were obtained using combined focused ion beam milling and scanning electron microscopy

151   (FIB/SEM). We used a Crossbeam® Neon40 EsB electron microscope with a field emission SEM

152   column and a Gallium FIB (Carl Zeiss NTS GmbH, Oberkochen, Germany). To select the exact

153   location to be imaged and to identify the cortical layers, we obtained semithin sections (2 μm

154   thick) from the block surface and stained them with toluidine blue. These sections were then

155   photographed with a light microscope. The last of these light microscope images

156   (corresponding to the section immediately adjacent to the block face) was then collated with

157   SEM photographs of the block face. A gallium ion beam was used to mill the sample, removing

158   thin layers of material on a nanometer scale. After removing each slice (20 nm thick), the

159   milling process was paused, and the freshly exposed surface was imaged with a 1.8-kV

160   acceleration potential using an in-column energy selective backscattered electron detector.

161   The milling and imaging processes were sequentially repeated in a fully automated way, and

162   long series of images were acquired, thus obtaining a stack of images that represented a 3-

163   dimensional sample of the tissue (Merchan-Perez et al., 2009). Twenty-nine different stacks of

164   images of the neuropil in the six layers of the somatosensory cortex were obtained (three

165   samples from layer I, four from layer II, ten from layer III, five from layer IV, three from layer V

166   and four from layer VI). All these stacks were used previously for the study of the density and

167   three-dimensional distribution of synapses (Anton-Sanchez et al., 2014; Merchan-Perez et al.,

168   2014), as well as for the quantitative estimation of the subcellular location of synapses on

169   spines and dendritic shafts (Santuy et al., 2017). This study was performed in the neuropil, so

170   we used stacks of images that did not contain cell somata or blood vessels. Image resolution in

171   the xy plane ranged from 3.7 to 4.5 nm/pixel. Resolution in the z axis (section thickness) was

172   20 nm. With these resolution parameters, we obtained images of 2048 x 1536 pixels, so the

173 field of view was 7.56 x 5.68 µm at 3.7 nm/pixel. Noise reduction was performed by line

174 averaging, and the acquisition time per image was approximately four minutes. Although the

175 resolution of FIB/SEM images can be increased, we chose these parameters as a compromise

176 solution to obtain a large enough field of view where synaptic junctions could still be clearly

177 identified, in a period of time that allowed us to acquire between 189 and 363 serial sections

178 per stack (mean: 254.66; total: 7385 sections).

179

180 *Extraction of the Synaptic Apposition Surface*

181

182 Synaptic junctions within these volumes were visualized and automatically segmented in three

183 dimensions with Espina software (Morales et al., 2011). The segmentation algorithm makes

184 use of the fact that presynaptic and postsynaptic densities appear as dark, electron-dense

185 structures under the electron microscope. It requires a Gaussian blur filter preprocessing step

186 to eliminate noisy pixels, followed by a gray-level threshold to extract all the voxels that fit the

187 gray levels of the synaptic junction. In this way, the resulting 3D segmentation includes both

188 the pre- and postsynaptic densities. Since the pre- and postsynaptic densities are located face

189 to face, their surface areas are very similar (correlation coefficients over 0.97; see (Schikorski

190 and Stevens, 1997, 1999). Thus, they can be simplified to a single surface and represented as

191 the surface of apposition between the pre- and postsynaptic densities. This surface can be

192 extracted from the three-dimensionally segmented synaptic junction (Morales et al., 2013). For

193 the sake of clarity, we will refer to this surface as the *synaptic apposition surface* (SAS). EspINA

194 was used to visualize the SAS in 3D and the possible presence of perforations or deep

195 indentations in the perimeter were recorded. EspINA was also used to measure SAS areas and

196 perimeters. Since the SAS adapts to the curvature of the synaptic junction, we have also

197 measured its curvature as one minus the ratio between the projected area of the SAS and the

198 area of the SAS. This measure would equal 0 in a totally flat SAS, and the value would increase

199 up to a maximum of 1 as the SAS curvature increases. All measurements have been corrected

200 for tissue shrinkage due to processing for electron microscopy (Merchan-Perez et al., 2009).

201 Correction factors for volume, surface and linear measurements were 0.73, 0.81 and 0.90,

202 respectively.

203

204 *Statistical analysis*

205 To study whether there were significant differences we performed multiple mean comparison

206 tests on the 29 samples of the six cortical layers. Since the necessary assumptions for ANOVA

207 were not satisfied (the normality and homoscedasticity criteria were not met), we used the

208 Mann-Whitney test for pair-wise comparisons. Chi-square tests were used for contingency

209 tables. Linear regression was used to find correlations. SPSS 22.0 (IBM Corp.) and Easyfit

210 Professional 5.5 (MathWave Technologies) were used.

211 **Results**

212

213 *Synaptic junction areas and perimeters*

214 In our samples, we found 7569 synaptic junctions. We discarded 678 (8.96%) because they

215 were truncated by the edges of the field of view. Thus, we finally analyzed 6891 synapses

216 whose synaptic junctions were complete, so their SAS could be extracted (Figure 1). Of these,

217 6259 (90.83%) were AS and 632 were SS (9.17%).

218 SAS areas ranged from 909.23 to 556393.19 nm^2 for AS, and from 3388.21 to 631774.04 nm^2

219 for SS. Mean SAS areas were smaller for AS than for SS in all cortical layers (Table 1, Figure 2A)

220 and these differences were statistically significant in all cases (MW tests, $p<0.001$ in layers I to

221 V and $p = 0.026$ in layer VI). For AS, the largest mean SAS areas were found in layer III (mean =

222 72729.58 nm^2) and the differences between this layer and all other layers were statistically

223 significant (MW, $p \leq 0.023$). The smallest mean SAS areas of AS were found in layer IV (mean =

224 54770.81 nm^2) and the differences between this layer and layers I, III and V were statistically

225 significant (MW, $p \leq 0.001$). For SS, the largest mean SAS areas were also found in layer III

226 (mean = 116703.43 nm^2; differences were statistically significant between this layer and layers

227 II, IV and VI; MW, $p \leq 0.002$). The smallest mean SAS areas of SS were found in layer IV (mean =

228 68355.35 nm^2) and the differences were statistically significant between this layer and all other

229 layers except layer VI (MW, $p \leq 0.031$).

230 We also measured the perimeters of the SAS (Table 2, Figure 2B). For each individual layer,

231 mean perimeters were always larger for SS than for AS (Figure 2B; Table 2). As expected, there

232 was a strong correlation between SAS area and perimeter ($R^2=0.75$ for all synapses; $R^2=0.75$ for

233 AS; $R^2=0.72$ for SS) (Figure 2C). It is also interesting to note that the larger the SAS area, the

234 more tortuous its perimeter. This can be seen in Figure 2C, which shows that the SAS

235 perimeter tends to grow faster than the perimeter of a circle.

236 To further characterize the size distribution of SAS, we plotted the frequency histograms of

237 SAS areas for each individual layer and for all layers as a whole. For AS, frequency histograms

238 had similar shapes in all layers, with a tail to the right, and they overlapped greatly (Figure 3A).

239 For SS, more irregular-shaped histograms were obtained for individual layers, probably due to

240 the smaller number of synaptic junctions that were analyzed per layer (Figure 3B) (see also

241 Table 1). We then performed goodness-of-fit tests to find the theoretical probability density

242 functions that best fitted the empirical distributions of SAS areas in each layer and in all layers

243 pooled together. We found that the best fit corresponded to log-normal distributions in all

244 cases (Table 1 and Figure 3). These log-normal distributions, with some variations in the

245 location (μ) and scale (σ) parameters (Table 1), were found in all layers for both AS and SS,

246 although the fit was better for AS than for SS, probably due to the smaller number of SS

247 analyzed (Figure 3). The best-fit probability density functions for SAS perimeters were also log-

248 normal distributions (Table 2).

249

250 *Size of synaptic junctions on dendritic spines and shafts*

251 We also determined whether the postsynaptic element where the synapses were established

252 (dendritic spines or shafts) was associated with differences in the size of PSDs. Unambiguous

253 identification of spines required the dendritic spine to be visually traced to the parent dendrite

254 within the 3D stack of serial sections. Similarly, dendritic shafts needed to be followed inside

255 the stack until they could be clearly identified. For this analysis, we studied 6000 synapses

256 whose postsynaptic targets were successfully identified. We found that the mean SAS area of

257 synapses located on dendritic shafts (88795.98 nm^2 ± sem = 2210.16) was larger than the

258 mean SAS area of those located on necks (57879.38 nm^2 ± sem= 3998.65) and spine heads

259 (65164.05 nm^2 ± sem= 797.26) (MW tests, p<0.001). This difference could be due to the fact

260 that SS, which are larger than AS, were predominantly located on dendritic shafts (in this

11

261   sample, 73.39% of SS were located on shafts, while only 14.61% of AS were located on shafts).

262   To rule out this possibility, we analyzed AS and SS independently. We found that the mean SAS

263   area of AS located on shafts (78255.07 nm^2 ± sem = 2413.73) was larger than those located on

264   dendritic spines heads (65196.81 nm^2 ± sem= 811.93) (MW test, p<0.001) and the ones on

265   spines heads were larger than those on necks (52326.09 nm^2 ± sem = 4394.36) (MW test,

266   p=0.04). Similarly, the mean SAS areas of SS were larger on shafts (109798.76 nm^2 ± sem=

267   4358.62) compared to dendritic spine heads (63808.43 nm^2 ± sem = 3592.90) and necks

268   (74697.93 nm^2 ± sem= 8576.53) (MW tests, p<0.001), although the difference between SS on

269   spine heads and necks was not statistically significant (MW tests, p=0.33). Therefore, synapses

270   located on dendritic shafts were larger than those located on dendritic spines, both for AS and

271   SS. When single cortical layers were analyzed, we also found that the mean SAS area of

272   synapses established on dendritic shafts was always larger than SAS areas of synapses on

273   dendritic spines. In spite of the differences in the mean SAS areas mentioned above, the

274   frequency histograms of SAS areas of AS and SS on dendritic shafts and spines greatly

275   overlapped, as shown in Figure 4.

276

277   *The shape of synaptic junctions*

278   The shape of synaptic junctions was very variable (Figure 5) but can be categorized into three

279   main types. Most cortical synapses had disc-shaped, macular PSDs (93%). A small percentage

280   had perforations, with one or more holes in the PSD (4.5%), while an even smaller proportion

281   (2.5%) had a tortuous horseshoe-shaped perimeter with an indentation. Macular and

282   perforated synapses followed the previously described 9:1 proportion between AS and SS, but

283   in the case of horseshoe-shaped PSDs, this proportion was 8:2, indicating that horseshoe-

284   shaped synaptic junctions were relatively more frequent among SS than among AS (Chi

285   squared, p< 0.001).

286   The mean SAS area of macular synapses was smaller (mean ± sem = 61737.72 nm^2 ± 606.10)

287   than horseshoe-shaped synapses (148469.66 nm^2 ± 6321.63) (MW test, p<0.001) and the

288   mean SAS area of horseshoe-shaped synaptic junctions was smaller than that of perforated

289   synapses (176710.07 nm^2 ± 5875.00) (MW test, p=0.005) (Table 3). Despite the differences in

290   the mean SAS areas, perforated and horseshoe-shaped synaptic junctions were intermingled

291   with the predominant macular synaptic junctions (Figures 5 and 6). The perimeter of macular

292   synapses was shorter (1423.96 nm ± 10.22) than horseshoe-shaped synapses (3124.70 nm ±

293   107.62) (MW test, p<0.001) and perforated synapses (3106.10 nm ± 87.94) (MW test,

294   p<0.001), while horseshoe-shaped and perforated synapses had similar perimeters (MW test,

295   p=0.59) (Table 3).

296   For all three categories (macular, perforated and horseshoe-shaped), SS had a larger area and

297   perimeter than AS (Table 3), although these differences were only statistically significant for

298   macular synapses (MW test; p<0.001).

299   The proportions of macular, horseshoe and perforated synaptic junctions were similar in layers

300   II to VI. However, we found that horseshoe-shaped and perforated synapses were more

301   common in layer I (Chi squared, p<0.001) (Figure 6A). No preference was found in the location

302   of macular, perforated or horseshoe-shaped synapses on spines or dendritic shafts — and this

303   was the case for both AS (Chi squared, p=0.22) and SS (Chi squared, p=0.66).

304   We also measured SAS curvature by calculating one minus the ratio between the projected

305   area of the SAS and the area of the SAS. This value would equal 0 for a totally flat SAS and it

306   would increase as the SAS becomes more curved or wrinkled (see Methods). Our results

307   indicate that SAS curvature was higher for SS than for AS in all layers (MW tests, p≤0.028)

308   (Figure 7A). We made pair comparisons of AS curvature between each cortical layer and all the

309   others and we found statistically significant differences between all layers (MW tests, p<0.05)

310   except between layers I and II (MW test, p=0.325), and layers III and V (MW test, p=0.14). For

311   SS, statistically significant differences were found between layers IV and VI (the ones with

312   flattest synapses) and all the other layers (MW tests, p<0.001). Macular synapses were flatter

313   (mean ± sem, 0.07 ± 0.001) than horseshoe-shaped (0.11 ± 0.005) (MW test, p<0.001) and

314   perforated synapses (0.10 ± 0.003) (MW test p<0.001). Horseshoe-shaped and perforated

315   synapses had similar curvature (MW test, p=0.58) (Table 3). We found no correlation between

316   SAS area and curvature (R^2 = 0.08 for AS; R^2 = 0.03 for SS) (Figure 7B).

317

Discussion

319   In the present study, we used a new method to estimate the size and shape of synapses that

320   involved extracting the SAS from synaptic junctions segmented in three dimensions, using

321   combined focused ion beam milling and scanning electron microscopy. This study provided

322   three main findings. Firstly, the mean SAS areas were smaller for AS than for SS in all cortical

323   layers and these differences were statistically significant in all cases. For both AS and SS, the

324   largest mean SAS areas were found in layer III and the smallest mean SAS areas were found in

325   layer IV. In all cases (AS and SS, in all layers), the distributions of synaptic junction size followed

326   a skewed curve with a long tail to the right, corresponding to a log-normal distribution.

327   Secondly, most cortical synapses had disc-shaped, macular PSDs (93%). A few were perforated,

328   with one or more holes in the PSD (4.5%), while an even smaller proportion (2.5%) showed a

329   tortuous horseshoe-shaped perimeter with a deep indentation. Thirdly, the SAS curvature was

330   larger for SS than for AS in all layers. However, there was no correlation between SAS area and

331   curvature for AS or SS.

332

333

334 *Methods to estimate the size of synaptic junctions*

335 Several methods have traditionally been used to estimate the size of synaptic junctions. The

336 simplest of these methods is to measure the cross-sectional length of synaptic junctions in

337 TEM micrographs. This method has obvious limitations since it is based on individual 2D

338 images where a portion of synapses cannot be fully characterized (for example, see DeFelipe et

339 al. (1999)), and it also reduces size estimation to a one-dimensional measurement that is not

340 equivalent to any easily interpretable geometrical measure such as the mean diameter, for

341 example. Methods that use serial sections can yield more reliable measurements, even if only

342 simple measurements such as the maximum width of the PSD are used (Tarusawa et al., 2009).

343 The cross-sectional length of the PSD can also be measured in each section of the series and

344 multiplied by section thickness and by number of sections (Arellano et al., 2007; Bopp et al.,

345 2017; Hsu et al., 2017). Alternatively, the PSD can be reconstructed from the series of sections

346 and its contour can be measured in 3D (Bosch et al., 2015; Dufour et al., 2015; Rollenhagen et

347 al., 2015; Bosch et al., 2016; Rodriguez-Moreno et al., 2017). Another measurement that has

348 been used to estimate the size of synaptic junctions in 3D is the diameter of Feret, which is

349 equivalent to the diameter of the smallest sphere circumscribing the reconstructed object

350 (Merchan-Perez et al., 2014). The Feret's diameter is a simple and reliable measurement that

351 can be automatically obtained at a low computational cost, and it has been shown to be useful

352 to build models that reproduce the distribution of synapses in three-dimensional space

353 (Anton-Sanchez et al., 2014). However, it does not accurately describe the morphology of

354 synapses, since it obviously oversimplifies the geometric characteristics of the measured

355 object, and it is clear that objects with very different morphologies can have similar Feret's

356 diameters. Another indirect measurement of the size of the synaptic junction is the axon-spine

357 interface (ASI), which represents the total apposition surface between the membrane of the

358 axonal bouton and the membrane of the dendritic spine (de Vivo et al., 2017). We have used

359 the synaptic apposition surface (SAS), which is equivalent to the interface between the active

360 zone and the PSD. Therefore, although the area of the ASI and the PSD are correlated

361 (Cheetham et al., 2014), data from de Vivo et al. (2017) are not comparable with ours, except

362 for the fact that our measurements of the SAS are smaller than their measurements of the ASI.

363 This is because the SAS is always inside the ASI and thus it is smaller than the ASI. Moreover,

364 our methodology provides information on the *shape* of the PSD, as well as information about

365 synapses established on dendritic shafts, that cannot be obtained from ASI measurements.

366 *Synaptic apposition surface*

367 In the present study, we used the synaptic apposition surface (SAS) because it has three main

368 advantages over the methods outlined above. First, it is extracted automatically from the

369 previously segmented synaptic junction with no user intervention, thus avoiding any manual

370 tracing of contours and possible associated user bias (Alonso-Nanclares et al., 2013; Morales et

371 al., 2013). Second, despite being a surface, the SAS is also a 3D object that adapts to, and

372 reproduces the shape and curvature of the PSD. Therefore, the SAS can be visualized in 3D to

373 obtain qualitative information such as the presence of perforations or indentations (see Figure

374 5). Third, quantitative information on the surface area, perimeter and curvature can also be

375 extracted from the SAS, so size and shape can easily be correlated. Given that the initial

376 segmentation of synaptic junctions has been performed within 3D tissue samples using a semi-

377 automatic method (Morales et al., 2011), and the SAS have been extracted in a fully

378 automated way, we have been able to obtain 6,891 synaptic junctions whose shape and size

379 have been analyzed in the six cortical layers. Additionally, the postsynaptic target (dendritic

380 spines or shafts) has been unambiguously identified in 6,000 of these synaptic junctions.

381 *Size of synaptic junctions*

382 The size of both types of synaptic junctions (asymmetric and symmetric) follows log-normal

383 distributions. Despite the fact that the mean SAS area is larger for SS than for AS, their

384 respective distributions greatly overlap (Figure 3), so it would be impossible to distinguish AS

16

385　from SS on the basis of synaptic junction size alone. It is tempting to correlate the log-normal

386　distribution of synaptic sizes with other parameters such as synaptic strength and spike

387　transmission probability, which also follow log-normal distributions (reviewed by Buzsaki and

388　Mizuseki (2014)). For example, the distribution of the size of unitary excitatory postsynaptic

389　potentials (EPSP) is very similar to the distribution of the size of SAS reported here, with a

390　skewed envelope and a long tail to the right (Song et al., 2005; Lefort et al., 2009). Moreover,

391　the EPSP amplitude strongly correlates with the number of postsynaptic AMPA receptors and

392　with spine head volume (Matsuzaki et al., 2001; Kasai et al., 2003; Araya, 2014), which in turn

393　strongly correlates with PSD size (Arellano et al., 2007). Model experiments also suggest that

394　PSD size has a strong influence on the activation of postsynaptic receptors (Montes et al.,

395　2015). It is also interesting to note that the event-to-event variability of synaptic strength for

396　individual synapses is largest for weaker synapses and decreases for stronger synapses (Lefort

397　et al., 2009; Ikegaya et al., 2013). This may also be related to synaptic junction size, since the

398　same phenomenon —a decrease in variability as synaptic size increases— has been described

399　in model experiments (Franks et al., 2002; Montes et al., 2015). This suggests that large

400　synapses have a higher number of receptors and are not only stronger, but also have a more

401　homogeneous and reliable response. However, it is important to note that the amplitude of

402　the EPSP also depends on the geometry of postsynaptic dendrites (Major et al., 2013; Eyal et

403　al., 2014), as well as on the morphology of dendritic spines (Gulledge et al., 2012; Araya, 2014).

404　Another important source of variability is the number of postsynaptic receptor molecules in

405　individual synapses. For example, it has been shown in the hippocampus that the number of

406　AMPA receptors as a function of synaptic size has different slopes in the synapses established

407　between Shaffer collaterals and CA1 dendritic spines and in the synapses between mossy

408　fibers and CA3 spines (Nusser et al., 1998). In the somatosensory cortex of the rat, AMPA

409　receptor concentration is similar in synapses of different sizes; thus, the larger the synapse the

410　higher the actual number of AMPA receptors (Kharazia and Weinberg, 1999), while NMDA

411   receptors are found at a higher concentration in smaller synapses. In any case, it is obvious

412   that the distribution of different types of receptors among different types of synapses is a

413   complex issue (Hadzic et al., 2017), so the relationship between synaptic size and receptor

414   number is not simple and requires further research.

415   Different synaptic sizes have been associated with different functions. For example, it has been

416   proposed that small dendritic spines are preferential sites for long-term potentiation

417   induction, whereas large spines might represent physical traces of long-term memory

418   (Matsuzaki et al., 2004; Kasai et al., 2010). Our data show that synaptic size follows a log-

419   normal distribution, which is unimodal and continuous, so neither AS nor SS can be divided

420   into two groups on the basis of synaptic junction size. Therefore, if the function of "learning or

421   memory" synapse depends on synaptic size, there would not be a clear-cut transition between

422   the two types of synapse. Additionally, It has been proposed that the functional role of

423   synapses may also depend on the sharp decrease of event-to-event variability as synaptic size

424   grows, so the functional transition between "learning and memory" synapses would be faster

425   than if it depended on synaptic size alone (Montes et al., 2015). In any case, if synapses of

426   different sizes serve different functions, synapses on dendritic shafts must also be taken into

427   account. Although such synapses are not the predominant type (about 15% of AS and 73% of

428   SS; see also (Santuy et al., 2017), their mean sizes are larger than axospinous synapses, both

429   for AS and SS.

430   *Horseshoe-shaped and perforated synapses*

431   Synaptic junctions with deep indentations (horseshoe synapses) and perforated synapses were

432   scarce in our sample; even if we pool together horseshoe-shaped and perforated synapses,

433   they only accounted for about 7% of the whole population. The question arises about whether

434   they are a separate population of synapses, with different morpho-functional features from

435   the predominant macular synapses. These types of synapses are mainly located in the right tail

436   of the synaptic size distributions, so their mean area is larger than the mean area of macular

437   synapses, in line with numerous studies (Calverley and Jones, 1987; Geinisman et al., 1987;

438   Jones and Calverley, 1991; Harris et al., 1992). Nevertheless, the sizes of horseshoe-shaped

439   and perforated synapses also greatly overlap with the sizes of macular synapses, so there is

440   not a boundary separating them from macular synapses (Fig. 6). Regarding the perimeter of

441   horseshoe and perforated synapses, again we did not find any boundary, since the perimeter

442   tends to be more complex as the PSD gets larger, regardless of the presence of perforations.

443   If we interpret perforations and deep indentations as dynamic, non-permanent, features that

444   may only depend on the molecular turnover of the constituents of the PSD, then perforated

445   and horseshoe PSDs would belong to the same pathway as macular PSDs. The smallest

446   synapses would have a macular shape whose perimeter would get progressively more tortuous

447   as they grow. Deep indentations and perforations would appear (and eventually disappear) as

448   the PSD becomes larger. The incorporation of receptors into the PSD depends on lateral

449   diffusion from the surrounding plasma membrane (Choquet and Triller, 2013; Li and Blanpied,

450   2016) and on processes of endocytosis and exocytosis from the endosomal compartment

451   (Choquet and Triller, 2013; Kneussel and Hausrat, 2016). In this scenario, we can hypothesize

452   that indentations and perforations could be the morphological correlate of a more active —or

453   just more apparent— turnover of receptors in larger PSDs. In fact, it has been shown in the

454   hippocampus that the relative proportions of horseshoe, perforated and fragmented or

455   partitioned synapses (synapses that have several irregular small disc-shaped PSDs, with no

456   connection between them) do change after the induction of long-term potentiation

457   (Geinisman et al., 1993; Toni et al., 2001). This phenomenon may or may not take place in the

458   neocortex, where we have found horseshoe and perforated PSDs but not partitioned synapses.

459   The fact that very different types of synapses such as AS and SS have perforations also

460   suggests that these perforations are the result of a general, non-specific mechanism, related to

461   synaptic growth and remodeling.

19

462   Alternatively, perforated and probably also horseshoe-shaped synaptic junctions may belong

463   to different populations of synapses. The main argument favoring this hypothesis is that in

464   certain terminals, specifically in thalamocortical boutons in layer IV, perforated synapses are

465   frequent (Bopp et al., 2017; Rodriguez-Moreno et al., 2017), while they are scarce if we

466   consider the whole synaptic population. Our data seems to contradict this hypothesis mainly

467   because the proportion of perforated synapses is very similar in layers II to VI. However,

468   thalamocortical synapses represent only a minor proportion of layer IV synapses (less than

469   10%; e.g., see da Costa and Martin (2009)) and, therefore, their number may not be high

470   enough to contribute to a significant difference with other layers. Species and age differences

471   must also be taken into consideration, since the proportion of perforated synapses in layer

472   II/III of the visual and frontal cortices of the adult mouse seem to be larger than those

473   reported here (Hsu et al., 2017).

474   *Curvature of the synaptic apposition surfaces.*

475   The relevance of the curvature of the synapse has been discussed since the seventies when

476   Jones and Devon (1978) described changes in the curvature when administering anesthetics.

477   Diverse studies led to the conclusion that positively curved synapses represented functional

478   synapses, while negatively curved synapses were non-functional. Later studies revoked this

479   view, as they showed that many other factors could influence the curvature of synapses (for

480   example, the region studied; positively curved synapses predominated in the cortex while

481   negatively curved synapses predominated in the hippocampus) (Calverley and Jones, 1990).

482   Nevertheless, more recent studies suggest that changes in the synaptic curvature may

483   influence synaptic efficacy (Medvedev et al., 2010). In the present study, we found that SAS

484   curvature was larger for SS than for AS in all layers. Furthermore, for AS, statistically significant

485   differences were found between all layers except between layers III and V. Curvature

486   differences between SS were found between layer IV and all the other layers, and this was also

487   the case for layer VI. Therefore, if synaptic curvature has an influence on synaptic efficacy, our

488   results would indicate that this characteristic is layer and synaptic-type dependent. However,

489   there was no correlation between SAS area and curvature for AS or SS. Since the area of the

490   SAS seems to be related to the strength of synapses, the significance of the differences in

491   synaptic curvature found between different layers and types of synapses observed in the

492   present study remains to be determined.

493   *Concluding remarks*

494   Collectively, the results indicate that there are laminar-specific similarities and differences

495   regarding the size and shape of synaptic junctions. The functional implication of these

496   variations is unknown but they may be related to synaptic attributes of particular synaptic

497   circuits which are characteristic of each layer. The data obtained in the present study is based

498   on the analysis of thousands of 3D-segmented synaptic junctions, providing a robust set of

499   morphological data. Since currently-available 3D quantitative data are rather scarce and

500   mainly based on individual cases, the present results in conjunction with other crucial

501   microanatomical data —such as the number and distribution of different types of synapses

502   and the identification of postsynaptic targets in different cortical layers— will help to better

503   understand the structure of microcircuits and to build realistic cortical models.

504

505

506   **References**

507   Alonso-Nanclares L, Gonzalez-Soriano J, Rodriguez JR, DeFelipe J (2008) Gender differences in

508   human cortical synaptic density. Proceedings of the National Academy of Sciences of

509   the United States of America 105:14615-14619.

510   Alonso-Nanclares L, Merino-Serrais P, Gonzalez S, DeFelipe J (2013) Synaptic changes in the

511   dentate gyrus of APP/PS1 transgenic mice revealed by electron microscopy. Journal of

512   Neuropathology & Experimental Neurology 72:386-395.

513   Anton-Sanchez L, Bielza C, Merchan-Perez A, Rodriguez JR, DeFelipe J, Larranaga P (2014)

514   Three-dimensional distribution of cortical synapses: a replicated point pattern-based

515   analysis. Front Neuroanat 8:85.

516   Araya R (2014) Input transformation by dendritic spines of pyramidal neurons. Front

517   Neuroanat 8:141.

518   Arellano JI, Benavides-Piccione R, Defelipe J, Yuste R (2007) Ultrastructure of dendritic spines:

519   correlation between synaptic and spine morphologies. Frontiers in Neuroscience

520   1:131-143.

521   Ascoli GA et al. (2008) Petilla terminology: nomenclature of features of GABAergic

522   interneurons of the cerebral cortex. Nature reviews Neuroscience 9:557-568.

523   Beaulieu C, Colonnier M (1985) A laminar analysis of the number of round-asymmetrical and

524   flat-symmetrical synapses on spines, dendritic trunks, and cell bodies in area 17 of the

525   cat. The Journal of comparative neurology 231:180-189.

526   Bopp R, Holler-Rickauer S, Martin KA, Schuhknecht GF (2017) An Ultrastructural Study of the

527   Thalamic Input to Layer 4 of Primary Motor and Primary Somatosensory Cortex in the

528   Mouse. Journal of Neuroscience 37:2435-2448.

529   Bosch C, Martinez A, Masachs N, Teixeira CM, Fernaud I, Ulloa F, Perez-Martinez E, Lois C,

530   Comella JX, DeFelipe J, Merchan-Perez A, Soriano E (2015) FIB/SEM technology and

531   high-throughput 3D reconstruction of dendritic spines and synapses in GFP-labeled

532   adult-generated neurons. Front Neuroanat 9:60.

533   Bosch C, Masachs N, Exposito-Alonso D, Martínez A, Teixeira CM, Fernaud I, Pujadas L, Ulloa F,

534   Comella JX, DeFelipe J, Merchán-Pérez A, Soriano E (2016) Reelin Regulates the

535   Maturation of Dendritic Spines, Synaptogenesis and Glial Ensheathment of Newborn

536   Granule Cells. Cerebral Cortex 26:4282-4298.

537   Branco T, Marra V, Staras K (2010) Examining size-strength relationships at hippocampal

538   synapses using an ultrastructural measurement of synaptic release probability. Journal

539   of structural biology 172:203-210.

540   Buzsaki G, Mizuseki K (2014) The log-dynamic brain: how skewed distributions affect network

541   operations. Nature Reviews Neuroscience 15:264-278.

542   Calverley RK, Jones DG (1987) A serial-section study of perforated synapses in rat neocortex.

543   Cell and tissue research 247:565-572.

544   Calverley RK, Jones DG (1990) Contributions of dendritic spines and perforated synapses to

545   synaptic plasticity. Brain research reviews 15:215-249.

546   Cheetham CE, Barnes SJ, Albieri G, Knott GW, Finnerty GT (2014) Pansynaptic enlargement at

547   adult cortical connections strengthened by experience. Cerebral Cortex 24:521-531.

548   Choquet D, Triller A (2013) The dynamic synapse. Neuron 80:691-703.

549   da Costa NM, Martin KA (2009) The proportion of synapses formed by the axons of the lateral

550   geniculate nucleus in layer 4 of area 17 of the cat. Journal of Comparative Neurology

551   516:264-276.

552   de Vivo L, Bellesi M, Marshall W, Bushong EA, Ellisman MH, Tononi G, Cirelli C (2017)

553   Ultrastructural evidence for synaptic scaling across the wake/sleep cycle. Science

554   355:507-510.

555   DeFelipe J, Fariñas I (1992) The pyramidal neuron of the cerebral cortex: morphological and

556   chemical characteristics of the synaptic inputs. Progress in Neurobiology 39:563-607.

557 DeFelipe J, Alonso-Nanclares L, Arellano JI (2002) Microstructure of the neocortex:
558   comparative aspects. Journal of neurocytology 31:299-316.

559 DeFelipe J, Marco P, Busturia I, Merchán-Pérez A (1999) Estimation of the Number of Synapses
560   in the Cerebral Cortex: Methodological Considerations. Cerebral Cortex 9:722-732.

561 Denk W, Horstmann H (2004) Serial block-face scanning electron microscopy to reconstruct
562   three-dimensional tissue nanostructure. PLoS biology 2:e329.

563 Dufour A, Rollenhagen A, Satzler K, Lubke JH (2015) Development of Synaptic Boutons in Layer
564   4 of the Barrel Field of the Rat Somatosensory Cortex: A Quantitative Analysis.
565   Cerebral Cortex.

566 Eyal G, Mansvelder HD, de Kock CP, Segev I (2014) Dendrites impact the encoding capabilities
567   of the axon. Journal of Neuroscience 34:8063-8071.

568 Fauth M, Tetzlaff C (2016) Opposing Effects of Neuronal Activity on Structural Plasticity. Front
569   Neuroanat 10:75.

570 Feldman ML (1984) Morphology of the neocortical Pyramidal neuron. In: Cerebral Cortex
571   (Peters A, Jones EG, eds), pp 123-200. New York: Plenum Press.

572 Franks KM, Bartol TM, Jr., Sejnowski TJ (2002) A Monte Carlo model reveals independent
573   signaling at central glutamatergic synapses. Biophysical journal 83:2333-2348.

574 Ganeshina O, Berry RW, Petralia RS, Nicholson DA, Geinisman Y (2004a) Synapses with a
575   segmented, completely partitioned postsynaptic density express more AMPA
576   receptors than other axospinous synaptic junctions. Neuroscience 125:615-623.

577 Ganeshina O, Berry RW, Petralia RS, Nicholson DA, Geinisman Y (2004b) Differences in the
578   expression of AMPA and NMDA receptors between axospinous perforated and
579   nonperforated synapses are related to the configuration and size of postsynaptic
580   densities. Journal of Comparative Neurology 468:86-95.

581 Geinisman Y, Morrell F, de Toledo-Morrell L (1987) Axospinous synapses with segmented
582   postsynaptic densities: a morphologically distinct synaptic subtype contributing to the

583   number of profiles of 'perforated' synapses visualized in random sections. Brain

584   research 423:179-188.

585   Geinisman Y, deToledo-Morrell L, Morrell F, Heller RE, Rossi M, Parshall RF (1993) Structural

586   synaptic correlate of long-term potentiation: formation of axospinous synapses with

587   multiple, completely partitioned transmission zones. Hippocampus 3:435-445.

588   Gulledge AT, Carnevale NT, Stuart GJ (2012) Electrical advantages of dendritic spines. PLoS One

589   7:e36007.

590   Hadzic M, Jack A, Wahle P (2017) Ionotropic glutamate receptors: Which ones, when, and

591   where in the mammalian neocortex. Journal of Comparative Neurology 525:976-1033.

592   Harris KM, Jensen FE, Tsao B (1992) Three-dimensional structure of dendritic spines and

593   synapses in rat hippocampus (CA1) at postnatal day 15 and adult ages: implications for

594   the maturation of synaptic physiology and long-term potentiation. Journal of

595   Neuroscience 12:2685-2705.

596   Helmstaedter M (2013) Cellular-resolution connectomics: challenges of dense neural circuit

597   reconstruction. Nature Methods 10:501-507.

598   Holderith N, Lorincz A, Katona G, Rozsa B, Kulik A, Watanabe M, Nusser Z (2012) Release

599   probability of hippocampal glutamatergic terminals scales with the size of the active

600   zone. Nature neuroscience 15:988-997.

601   Houser CR, Vaughn JE, Hendry SHC, Jones EG, Peters A (1984) GABA neurons in cerebral cortex.

602   Functional Properties of Cortical Cells. In: Cerebral Cortex (Peters A, Jones EG, eds), pp

603   63-89. New York: Plenum Press.

604   Hsu A, Luebke JI, Medalla M (2017) Comparative ultrastructural features of excitatory synapses

605   in the visual and frontal cortices of the adult mouse and monkey. Journal of

606   Comparative Neurology 525:2175-2191.

607 Ikegaya Y, Sasaki T, Ishikawa D, Honma N, Tao K, Takahashi N, Minamisawa G, Ujita S, Matsuki
608   N (2013) Interpyramid spike transmission stabilizes the sparseness of recurrent
609   network activity. Cerebral Cortex 23:293-304.

610 Jones DG, Devon RM (1978) An ultrastructural study into the effects of pentobarbitone on
611   synaptic organization. Brain research 147:47-63.

612 Jones DG, Calverley RK (1991) Perforated and non-perforated synapses in rat neocortex: three-
613   dimensional reconstructions. Brain research 556:247-258.

614 Kasai H, Matsuzaki M, Noguchi J, Yasumatsu N, Nakahara H (2003) Structure-stability-function
615   relationships of dendritic spines. Trends Neurosci 26:360-368.

616 Kasai H, Fukuda M, Watanabe S, Hayashi-Takagi A, Noguchi J (2010) Structural dynamics of
617   dendritic spines in memory and cognition. Trends Neurosci 33:121-129.

618 Kharazia VN, Weinberg RJ (1999) Immunogold localization of AMPA and NMDA receptors in
619   somatic sensory cortex of albino rat. Journal of Comparative Neurology 412:292-302.

620 Kneussel M, Hausrat TJ (2016) Postsynaptic Neurotransmitter Receptor Reserve Pools for
621   Synaptic Potentiation. Trends Neurosci 39:170-182.

622 Knott G, Marchman H, Wall D, Lich B (2008) Serial section scanning electron microscopy of
623   adult brain tissue using focused ion beam milling. Journal of Neuroscience 28:2959-
624   2964.

625 Lefort S, Tomm C, Floyd Sarria JC, Petersen CC (2009) The excitatory neuronal network of the
626   C2 barrel column in mouse primary somatosensory cortex. Neuron 61:301-316.

627 Li TP, Blanpied TA (2016) Control of Transmembrane Protein Diffusion within the Postsynaptic
628   Density Assessed by Simultaneous Single-Molecule Tracking and Localization
629   Microscopy. Frontiers in synaptic neuroscience 8:19.

630 Lisman J (2017) Glutamatergic synapses are structurally and biochemically complex because of
631   multiple plasticity processes: long-term potentiation, long-term depression, short-term

632   potentiation and scaling. Philosophical Transactions of the Royal Society B: Biological

633   Sciences 372.

634 Major G, Larkum ME, Schiller J (2013) Active properties of neocortical pyramidal neuron

635   dendrites. Annual Review of Neuroscience 36:1-24.

636 Markram H et al. (2015) Reconstruction and Simulation of Neocortical Microcircuitry. Cell

637   163:456-492.

638 Matsuzaki M, Honkura N, Ellis-Davies GCR, Kasai H (2004) Structural basis of long-term

639   potentiation in single dendritic spines. Nature 429:761-766.

640 Matsuzaki M, Ellis-Davies GC, Nemoto T, Miyashita Y, Iino M, Kasai H (2001) Dendritic spine

641   geometry is critical for AMPA receptor expression in hippocampal CA1 pyramidal

642   neurons. Nature neuroscience 4:1086-1092.

643 Matz J, Gilyan A, Kolar A, McCarvill T, Krueger SR (2010) Rapid structural alterations of the

644   active zone lead to sustained changes in neurotransmitter release. Proceedings of the

645   National Academy of Sciences of the United States of America 107:8836-8841.

646 Medvedev NI, Popov VI, Dallerac G, Davies HA, Laroche S, Kraev IV, Rodriguez Arellano JJ,

647   Doyere V, Stewart MG (2010) Alterations in synaptic curvature in the dentate gyrus

648   following induction of long-term potentiation, long-term depression, and treatment

649   with the N-methyl-D-aspartate receptor antagonist CPP. Neuroscience 171:390-397.

650 Merchan-Perez A, Rodriguez JR, Alonso-Nanclares L, Schertel A, DeFelipe J (2009) Counting

651   synapses using FIB/SEM microscopy: a true revolution for ultrastructural volume

652   reconstruction. Front Neuroanat 3:14.

653 Merchan-Perez A, Rodriguez JR, Gonzalez S, Robles V, Defelipe J, Larranaga P, Bielza C (2014)

654   Three-dimensional spatial distribution of synapses in the neocortex: a dual-beam

655   electron microscopy study. Cerebral Cortex 24:1579-1588.

656 Montes J, Pena JM, DeFelipe J, Herreras O, Merchan-Perez A (2015) The influence of synaptic

657   size on AMPA receptor activation: a Monte Carlo model. PLoS One 10:e0130924.

27

658 Morales J, Rodriguez A, Rodriguez JR, DeFelipe J, Merchan-Perez A (2013) Characterization and

659   extraction of the synaptic apposition surface for synaptic geometry analysis. Front

660   Neuroanat 7:10.

661 Morales J, Alonso-Nanclares L, Rodriguez J-R, Defelipe J, Rodriguez A, Merchan-Perez A (2011)

662   Espina: a tool for the automated segmentation and counting of synapses in large

663   stacks of electron microscopy images. Front Neuroanat 5:18.

664 Morgan JL, Lichtman JW (2013) Why not connectomics? Nature Methods 10:494-500.

665 Nusser Z, Lujan R, Laube G, Roberts JD, Molnar E, Somogyi P (1998) Cell type and pathway

666   dependence of synaptic AMPA receptor number and variability in the hippocampus.

667   Neuron 21:545-559.

668 Paxinos G, Watson C (2007) The Rat Brain in Stereotaxic Coordinates. In, 6th Edition: Academic

669   Press.

670 Peters A, Palay SL, Webster HD (1991) The fine structure of the nervous system: The neurons

671   and supporting cells., 3rd edition Edition. New York: Oxford University Press.

672 Rodriguez-Moreno J, Rollenhagen A, Arlandis J, Santuy A, Merchan-Perez A, DeFelipe J, Lübke

673   J, Clasca F (2017) Quantitative 3D ultrastructure of synaptic boutons from the

674   'lemniscal' ventral posteromedial thalamic nucleus in mouse barrel cortex. Submitted.

675 Rollenhagen A, Klook K, Satzler K, Qi G, Anstotz M, Feldmeyer D, Lubke JH (2015) Structural

676   determinants underlying the high efficacy of synaptic transmission and plasticity at

677   synaptic boutons in layer 4 of the adult rat 'barrel cortex'. Brain Structucture and

678   Function 220:3185-3209.

679 Santuy A, Rodriguez J, DeFelipe J, Merchan-Perez A (2017) Volume electron microscopy of the

680   distribution of synapses in the juvenile rat somatosensory cortex. Submitted.

681 Schikorski T, Stevens CF (1997) Quantitative ultrastructural analysis of hippocampal excitatory

682   synapses. Journal of Neuroscience 17:5858-5867.

683   Schikorski T, Stevens CF (1999) Quantitative fine-structural analysis of olfactory cortical

684   synapses. Proceedings of the National Academy of Sciences of the United States of

685   America 96:4107-4112.

686   Schüz A, Palm G (1989) Density of neurons and synapses in the cerebral cortex of the mouse.

687   Journal of Comparative Neurology 286:442-455.

688   Silberberg G (2008) Polysynaptic subcircuits in the neocortex: spatial and temporal diversity.

689   Current opinion in neurobiology 18:332-337.

690   Smith SJ (2007) Circuit reconstruction tools today. Current opinion in neurobiology 17:601-608.

691   Song S, Sjostrom PJ, Reigl M, Nelson S, Chklovskii DB (2005) Highly nonrandom features of

692   synaptic connectivity in local cortical circuits. PLoS biology 3:e68.

693   Takumi Y, Ramirez-Leon V, Laake P, Rinvik E, Ottersen OP (1999) Different modes of expression

694   of AMPA and NMDA receptors in hippocampal synapses. Nature neuroscience 2:618-

695   624.

696   Tarusawa E, Matsui K, Budisantoso T, Molnar E, Watanabe M, Matsui M, Fukazawa Y,

697   Shigemoto R (2009) Input-specific intrasynaptic arrangements of ionotropic glutamate

698   receptors and their impact on postsynaptic responses. Journal of Neuroscience
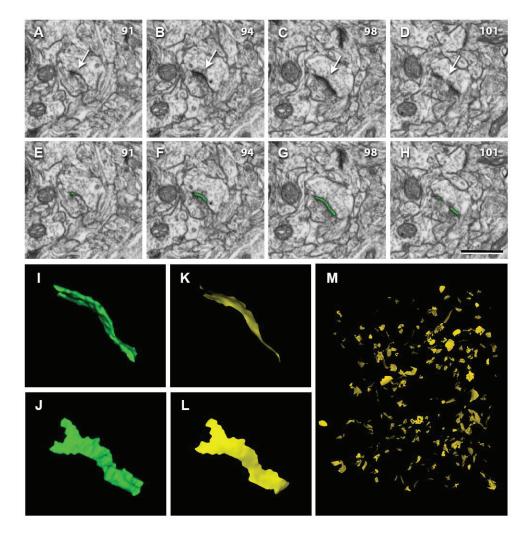
699   29:12896-12908.

700   Toni N, Buchs PA, Nikonenko I, Povilaitite P, Parisi L, Muller D (2001) Remodeling of synaptic

701   membranes after induction of long-term potentiation. Journal of Neuroscience

702   21:6245-6251.

703   White EL (2007) Reflections on the specificity of synaptic connections. Brain research reviews

704   55:422-429.

705   White EL, Keller A (1989) Cortical Circuits: Synaptic Organization of the Cerebral Cortex.

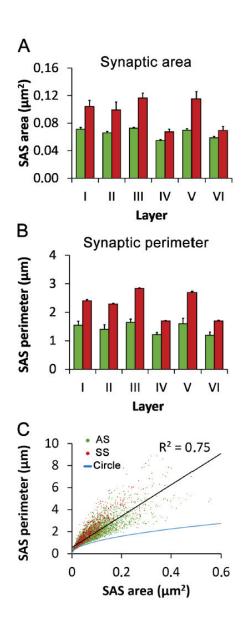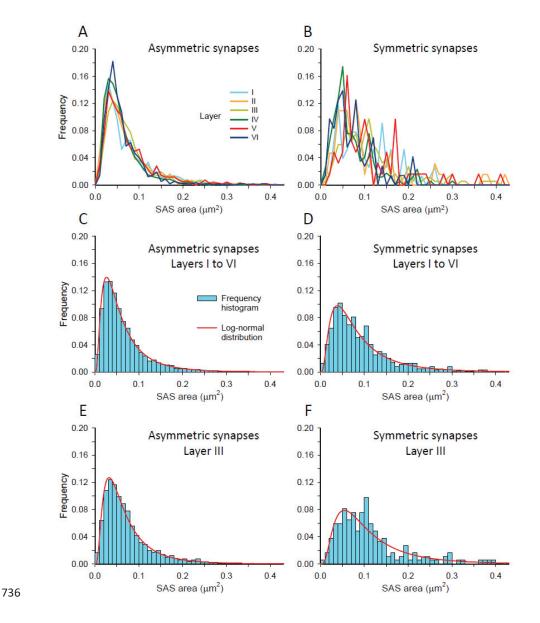706   Structure, Function and Theory. Boston: Birkhäuser.

707

Figures

709

710 **Figure 1**. **Identification, segmentation and extraction of the synaptic apposition surface (SAS)**
711 **of a synaptic junction from serial images obtained with combined Focused Ion Beam milling**
712 **and Scanning Electron Microcopy (FIB/SEM).** (A-D) Sections 91, 94, 98 and 101 from a stack of
713 serial sections obtained with FIB/SEM from the rat somatosensory cortex. Identification of an
714 asymmetric synapse whose prominent postsynaptic density is clearly visible (arrow). Note that
715 the identification was not based on single images but on the examination of the full sequence
716 of images where the synapse was visible (numbers in the top-right corner of each frame
717 correspond to section number; each individual section was 20 nm thick). (E-H) Segmentation of
718 the synaptic junction (green) with Espina software. (I, J) The resulting 3D object representing
719 the synaptic junction (green) visualized from two different angles. (K, L) The SAS (yellow) that
720 has been extracted from the 3D synaptic junction shown in (I) and (J). (M) Panoramic view of
721 all the SAS extracted from a whole stack of images. Scale bar in (H): 1μm for (A-H).

722

Figure 2. Size and perimeter of synaptic junctions (mean ± sem)**.** (A) Surface area of synaptic apposition surfaces (SAS) of asymmetric synapses (AS, green bars) and symmetric synapses (SS, red bars) in the six cortical layers. AS were smaller than SS in all layers (MW tests, p<0.001 in layers I to V; p=0.026 in layer VI). For both AS and SS, the largest SAS were found in layer III and the smallest were found in layer IV. (B) Perimeters of SAS of AS (green bars) and SS (red bars) in the six cortical layers. Perimeters of SAS showed similar differences to SAS areas. (C) Scatter plot showing the relationship between SAS areas and perimeters. AS are represented as green dots and SS as red dots. The blue trace indicates the perimeter/area relation of a circle, as a reference. There is a strong correlation between SAS area and perimeter (R^2=0.75 for AS and SS pooled together, black trace). If we compare the perimeter/area relation of a circle (blue trace) with the SAS perimeter/area plot of SAS, it is clear that SAS perimeters grow faster than the perimeter of a circle, indicating that SAS perimeters tend to be more tortuous as SAS area increases.

Figure 3. Frequency histograms of SAS areas and their corresponding best-fit probability density functions. Frequency histograms of SAS areas in the six cortical layers are represented for AS and SS in (A) and (B), respectively. Histograms for AS from different layers had similar shapes and overlapped greatly, while histograms for SS were more irregular. AS and SS from all layers have been pooled together to build the frequency histograms (blue bars) represented in (C) and (D). The best-fit distributions representing the theoretical probability density functions (red traces) have been represented with their corresponding frequency histograms. As an example for an individual layer, histograms and best-fit distributions for AS and SS from layer III have been represented in (E) and (F). The best-fit probability function was a log normal distribution in all cases. Curve fitting was always better for AS (C and E) than for SS (D and F), probably because of the smaller sample size of SS (see Table 1). The parameters μ and σ of the log-normal curves are shown in Table 1.
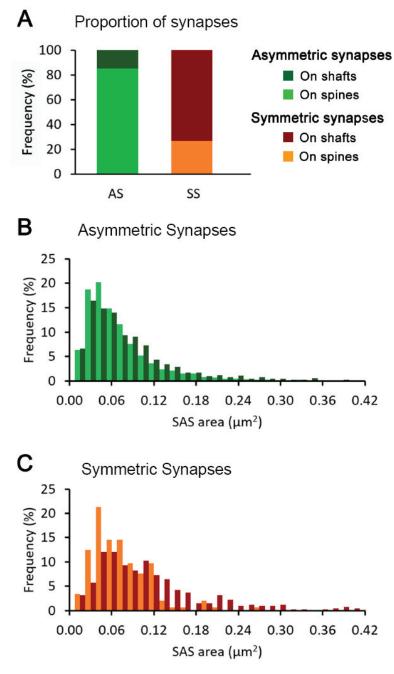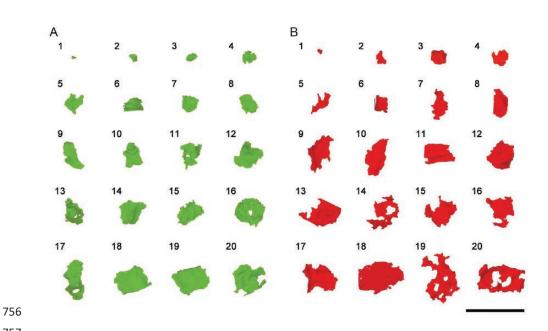
A Proportion of synapses

Asymmetric synapses
- On shafts
- On spines

Symmetric synapses
- On shafts
- On spines

B Asymmetric Synapses

C Symmetric Synapses

749

750 **Figure 4. SAS areas of synapses on dendritic spines and shafts. (A)** Proportions of asymmetric
751 and symmetric synapses on dendritic spines and shafts. **(B)** Frequency histograms of SAS areas
752 of asymmetric synapses on dendritic spines (light green) and on dendritic shafts (dark green).
753 **(C)** Frequency histograms of SAS areas of symmetric synapses on dendritic spines (orange) and
754 on dendritic shafts (dark orange). Frequencies in (B) and (C) have been normalized for each
755 individual category.

756

757

Figure 5. Representative sample of synaptic apposition surfaces of asymmetric and symmetric synapses. (A) Synaptic apposition surfaces of asymmetric synapses (green) were distributed into 20 bins of equal size. An example within each bin has been represented here. **(B)** Synaptic apposition surfaces of symmetric synapses (red) that were distributed and selected as in (A). Calibration bar = 1μm.
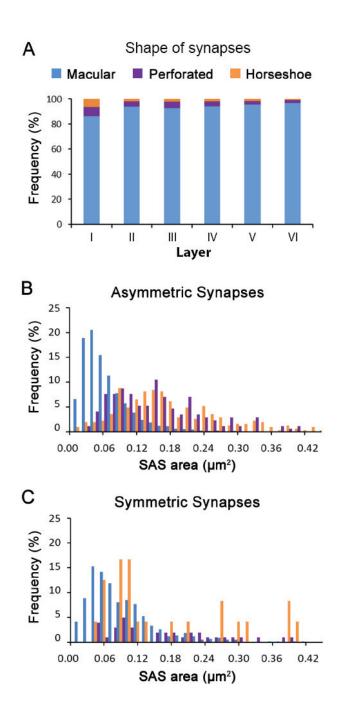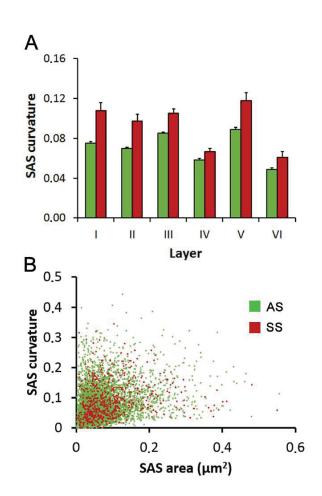
763

Figure 6. **Distribution of synapses of different shapes. (A)** Proportion of macular (blue), perforated (purple) and horseshoe-shaped (orange) synapses in the six layers of the cortex. Layer I shows a higher proportion of perforated and horseshoe synapses when compared to layers II-VI (Chi squared, p<0.001). **(B)** Frequency histograms of the SAS area of macular, perforated and horseshoe-shaped asymmetric synapses. **(C)** Frequency histograms of the SAS area of macular, perforated and horseshoe-shaped symmetric synapses. Frequencies in (B) and (C) have been normalized for each individual category.

771

Figure 7. Curvature of the synaptic apposition surfaces (SAS). **(A)** SAS curvature of AS and SS in the six cortical layers (mean ± sem). SAS curvature was larger for SS (red bars) than for AS (green bars) in all layers. For AS, statistically significant differences were found between all layers (MW tests <0.05) except between layers I and II (MW test, p=0.325) and layers III and V (MW test, p=0.14). Curvature differences between SS were found between layers IV and VI and all the other layers (MW tests, p<0.001). **(B)** Scatter plot representing the relationship between SAS curvature and area of AS (green dots) and SS (red dots). There was no correlation between SAS area and curvature for AS or SS (R^2 = 0.08 for AS; R^2 = 0.03 for SS).

780

781 **Tables**

782

	AS				SS			
	Mean SAS area ± sem (nm^2)	n	μ	σ	Mean SAS area ± sem (nm^2)	n	μ	σ
Layer I	70834.87 ±	594	10.81	0.88	104309.94 ±	77	11.29	0.78
Layer II	58987.37 ±	992	10.72	0.83	87757.53 ±	64	11.14	0.72
Layer III	72729.58 ±	2212	10.93	0.74	116703.42 ±	185	11.42	0.72
Layer IV	54770.81 ±	1200	10.65	0.73	68355.35 ±	172	10.88	0.73
Layer V	69682.16 ±	684	10.85	0.81	113353.40±	62	11.41	0.69
Layer VI	58668.28 ±	577	10.73	0.70	69382.12 ±	72	10.90	0.76
Layers I-VI	65299.31±	6259	10.84	0.79	93384.53 ±	632	11.17	0.78

783

784 **Table 1.** Mean synaptic apposition surface (SAS) area (nm^2 ± sem), number of synaptic SAS

785 analyzed (n), and the location (μ) and scale (σ) of the best-fit log-normal distributions in the six

786 cortical layers. Unweighted means for layers I to VI are also given. AS: asymmetric synapses;

787 SS: symmetric synapses.

788

789

	AS				SS			
	Mean SAS perimeter ± sem (nm)	n	μ	σ	Mean SAS perimeter ± sem (nm)	n	μ	σ
Layer I	1538.03 ± 42.13	594	7.16	0.60	2405.01 ± 142.87	77	7.65	0.55
Layer II	1365.80 ± 29.46	992	7.06	0.55	2141.62 ± 130.11	64	7.55	0.52
Layer III	1638.51 ± 19.64	2212	7.27	0.59	2838.22 ± 118.19	185	7.81	0.54
Layer IV	1221.79 ± 18.70	1200	6.99	0.47	1704.83 ± 77.28	172	7.29	0.54
Layer V	1602.44 ± 38.50	684	7.22	0.56	2736.41 ± 186.46	62	7.77	0.50
Layer VI	1191.59 ± 25.83	577	6.97	0.45	1697.00 ± 112.65	72	7.29	0.55
Layers I-VI	1460.71 ± 11.29	6259	7.14	0.54	2266.44 ± 54.61	632	7.56	0.59

790

791 **Table 2.** Mean SAS perimeter (nm ± sem), number of synapses analyzed (n), and the location

792 (μ) and scale (σ) of the log-normal distributions of SAS perimeters in the six cortical layers.

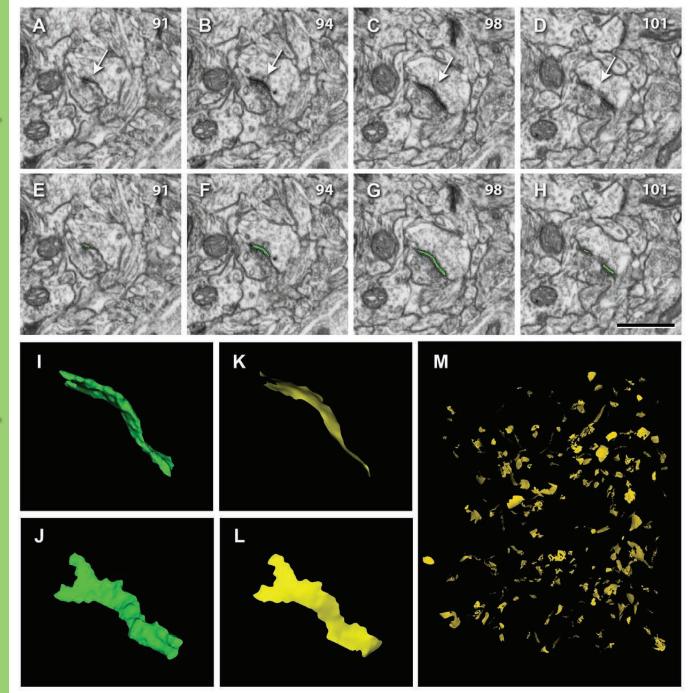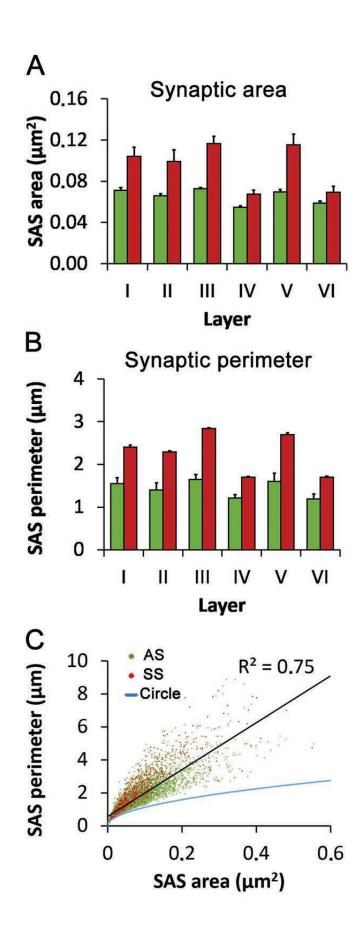793 Unweighted means for layers I to VI are also shown. AS: asymmetric synapses; SS: symmetric

794 synapses.

795

796

Shape of synaptic junction	Type of synapse	Area of SAS (nm^2) mean ± sem	Perimeter (nm) mean ± sem	Curvature mean ± sem
Macular	AS	59271.15 ± 595.95	1353.95 ± 9.55	0.07 ± 0.001
	SS	86903.65 ± 2816.34	2138.30 ± 51.47	0.09 ± 0.003
	AS+SS	61737.72 ± 606.10	1423.96 ± 10.22	0.07 ± 0.001
Perforated	AS	175955.57 ± 5842.02	3056.56 ± 85.68	0.10 ± 0.004
	SS	185606.8 ± 30594.69	3690.38 ± 488.31	0.08 ± 0.010
	AS+SS	176710.07 ± 5875.00	3106.10 ± 87.94	0.10 ± 0.003
Horseshoe-shaped	AS	146689.44 ± 6756.57	3015.70 ± 109.07	0.11 ± 0.006
	SS	155387.11 ± 16435.88	3548.22 ± 304.55	0.08 ± 0.009
	AS+SS	148469.66 ± 6321.63	3124.70 ± 107.62	0.11 ± 0.005

797

798   **Table 3.** Area (nm2), perimeter (nm) and curvature (mean ± sem) of the SAS of macular,

799   perforated and horseshoe-shaped synaptic junctions. AS: asymmetrical synapses; SS:

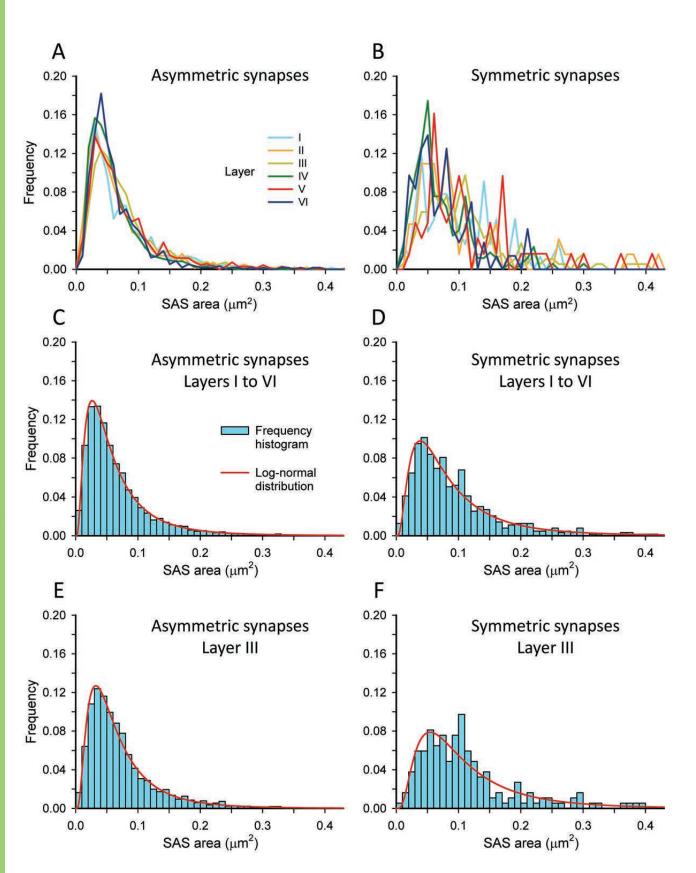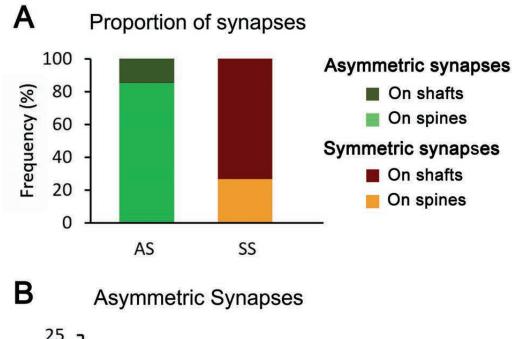800   symmetrical synapses. All data are given as mean ± sem.

A **Synaptic area**

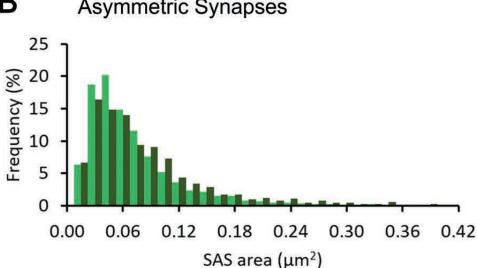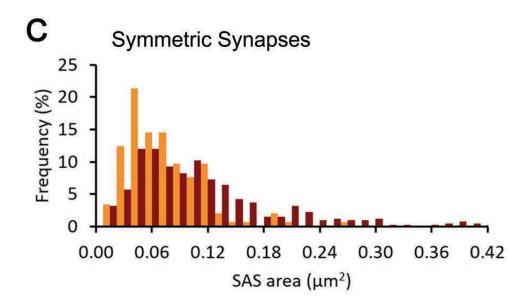B **Synaptic perimeter**

C

A   Proportion of synapses

Asymmetric synapses
- On shafts
- On spines

Symmetric synapses
- On shafts
- On spines

B   Asymmetric Synapses

C   Symmetric Synapses

A

1	2	3	4
5	6	7	8
9	10	11	12
13	14	15	16
17	18	19	20

B

1	2	3	4
5	6	7	8
9	10	11	12
13	14	15	16
17	18	19	20

A Shape of synapses

■ Macular ■ Perforated ■ Horseshoe

B Asymmetric Synapses

C Symmetric Synapses